HHS Public Access

Author manuscript

Nat Neurosci. Author manuscript; available in PMC 2016 March 01.

Published in final edited form as:

Nat Neurosci. 2015 March ; 18(3): 393–401. doi:10.1038/nn.3946.

Sensory inputs control the integration of neurogliaform interneurons into cortical circuits

Natalia V De Marco García[1,2,3,4], **Rashi Priya**[1,2,3], **Sebnem N Tuncdemir**[1,2,3], **Gord Fishell**[1,2,3], and **Theofanis Karayannis**[1,2,3]

[1]NYU Neuroscience Institute, New York Langone Medical Center, New York, New York, USA

[2]Department of Neuroscience and Physiology, New York Langone Medical Center, New York, New York, USA

[3]Department of Neural Science, New York University, New York, New York, USA

Abstract

Neuronal microcircuits in the superficial layers of the mammalian cortex provide the substrate for associative cortical computation. Inhibitory interneurons constitute an essential component of the circuitry and are fundamental to the integration of local and long-range information. Here we report that, during early development, superficially positioned Reelin-expressing neurogliaform interneurons in the mouse somatosensory cortex receive afferent innervation from both cortical and thalamic excitatory sources. Attenuation of ascending sensory, but not intracortical, excitation leads to axo-dendritic morphological defects in these interneurons. Moreover, abrogation of the NMDA receptors through which the thalamic inputs signal results in a similar phenotype, as well as in the selective loss of thalamic and a concomitant increase in intracortical connectivity. These results suggest that thalamic inputs are critical in determining the balance between local and long-range connectivity and are fundamental to the proper integration of Reelin-expressing interneurons into nascent cortical circuits.

The ability of the neocortex to process sensory information and transform it into meaningful motor output depends on functional neural circuits involving a diversity of cell types. At the microcircuit level, neurons face the challenge of integrating peripheral sensory information and recurrent local cortical activity. Indeed, the maintenance of a proper balance between cortical and thalamic inputs is fundamental to information processing because the former inputs regulate the gain of thalamic excitation[1]. However, the mechanisms by which the formation of these complex cortical circuits is regulated, including the establishment and

Correspondence should be addressed to G.F. (fisheg01@nyumc.org).

[4]Present address: Brain and Mind Research Institute, Weill Cornell Medical College, New York, New York, USA.

Note: Any Supplementary Information and Source Data files are available in the online version of the paper.

AUTHOR CONTRIBUTIONS

N.V.D.M.G., T.K. and G.F. conceived the project. N.V.D.M.G., T.K. and R.P. performed the experiments. S.N.T. prepared the rabies virus. N.V.D.M.G. wrote the manuscript with the help of all authors.

COMPETING FINANCIAL INTERESTS

The authors declare no competing financial interests.

maintenance of an appropriate balance between thalamic and intracortical inputs, are unknown.

Recent work has highlighted the importance of interneurons in the superficial layers of the cortex for cortical computation. Indeed, these neurons are strategically positioned to receive feedforward inputs from the thalamus and feedback inputs from the cortex. Superficial cortical interneurons, delineated by Reelin (Re) or vasointestinal peptide (VIP) expression, constitute approximately 30% of the total number of interneurons in the mouse brain and 50% in the human brain[2,3]. The increase in abundance of this population across species is speculated to reflect the larger demand for associative functions in the human brain[3]. In the mouse, superficial cortical interneurons have been shown both to participate in local disinhibitory circuits[4,5] and to control the transfer of long-range information from the motor cortex[6], contralateral hemisphere[7] and amygdala[8]. Despite the central role of these interneurons in cortical function, the developmental steps that regulate the establishment of their specific connectivity patterns are not understood. In an effort to understand the contribution of activity to interneuron development, we compared in a preceding study how dampening excitation of interneurons at particular developmental time points affected the positioning and maturation of specific interneuron subtypes[9]. We observed marked differences in the requirement for activity in VIP multipolar cells, which were apparently unaffected by attenuated levels of excitation, unlike Re^+ neurogliaform cells, whose migration and morphological development were markedly impaired[9]. Despite discovering a requirement for activity for the development of Re^+ neurogliaform cells, the presynaptic source and the neurotransmitter used, as well as receptor(s) required for this process, all remained unknown.

To begin to assess whether aspects of the developing circuit play a role in the proper integration of Re^+ interneurons, we here examined the early connectivity of this subtype using a modified version of the rabies-based monosynaptic tracing method[10]. Although layer IV has been classically regarded as the primary recipient of ascending sensory information carried via thalamic terminals[11], we found, unexpectedly, that during the first postnatal week, in addition to inputs from intracortical sources, Re^+ interneurons in layers I–III also receive direct thalamic inputs.

Notably, presynaptic interference with thalamic but not intracortical inputs impaired the morphological development of Re^+ interneurons. In exploring the mechanisms underlying this observation, we found that thalamocortical synapses use NMDA receptors (NMDARs) containing the NR2B subunit and that cell-autonomous removal of these receptors (but not NR2A-containing receptors) led to severe morphological defects in Re^+ interneurons. Strikingly, in the absence of NMDAR-mediated currents, the ratio of thalamocortical to intracortical innervation was dramatically altered such that a concomitant increase in intracortical innervation occurred at the expense of thalamic afferents (Supplementary Fig. 1). Our results indicate that ascending excitatory thalamic activity controls the balance of afferents impinging on select subtypes of superficial layer interneurons.

RESULTS

Mapping the anatomical connectivity of developing cortical Re+ neurogliaform interneurons

Mature neurogliaform interneurons located in the superficial layers of the somatosensory cortex receive innervation from local pyramidal cells and GABAergic interneurons[12]. However, how this pattern of innervation develops is unknown. To determine the development pattern of afferent connectivity to these interneurons, we adapted the monosynaptic rabies tracing technique[10,13,14] such that we could target individual Re$^+$ interneurons. We electroporated at embryonic day (E) 15.5 a construct in which the expression of a histone2B.eGFP (hGFP) fusion protein reporter, TVA800 receptor and B19G glycoprotein was directed to interneurons through the use of an *Dlx5/6* enhancer element[9] (Dlx5/6-hGFP-TVA-B19G). Monosynaptic tracing of the afferents to this population was achieved through stereotactic injection of a recombinant rabies virus (SADΔG_mCherry(EnvA)) into the somatosensory barrel field 1 area (SSBF1) at postnatal day (P) 3, followed by analysis at P8–P10 (Fig. 1a and Supplementary Fig. 2). The focal rabies injection together with the sparse electroporation of ventrally generated interneurons further diluted by their dispersion during tangential migration to the cortex[15] allowed us to target one starter cell in each experimental brain (Fig. 1a–d and Supplementary Fig. 2). Thus, this technique allowed us to map the afferent connectivity to individual Re$^+$ interneurons during early postnatal periods. The identity of starter cells and presynaptic targets was confirmed through immunohistochemistry of excitatory cell and interneuron markers, combined with analysis of their morphological features (Supplementary Fig. 2; see also Online Methods). We found that each Re$^+$ interneuron received inputs from 196 ± 48 (s.e.m.) presynaptic neurons located in cortical and subcortical structures. Surprisingly, a considerable proportion of these inputs originated in the ventroposteromedial (VPM) and posteromedial (POm) nuclei of the thalamus (VPM and POm: 56 o 6%). In addition, Re$^+$ interneurons received local afferents from pyramidal and subplate cells (14 ± 2%), as well as from other interneurons (30 ± 8%) (Fig. 1c). Notably, unlike in other interneuron populations we have investigated, such as VIP- and SST-expressing interneurons (Supplementary Fig. 3 and data not shown), we did not observe appreciable inputs onto the Re$^+$ interneurons from ascending neuromodulatory fibers such as those from the dorsal raphe and the nucleus basalis (although, on the basis of our previous findings[16], we infer such innervation must ultimately be established). As our previous experimental findings had suggested a prominent role for glutamatergic activity in driving the integration of Re$^+$ interneurons into cortical circuits[9], we focused our studies on the contributions of thalamic and intracortical excitatory afferents.

Re+ interneurons receive functional connectivity from somatosensory thalamic nuclei

To confirm that the anatomical pattern of connectivity revealed by the retrograde monosynaptic tracing corresponds to functional connectivity, we carried out channelrhodopsin-2 (ChR2)-assisted optogenetic mapping. To direct the expression of ChR2 to cortical pyramidal cells, we used *Emx1^{Cre}* or *Bhlhb5^{Cre}* (*Bhlhe22^{Cre}*) mouse driver lines in combination with a *loxP.Stop.loxP* (*LSL*) ChR2 (*Rosa26$^{LSL.ChR2\text{-}EYFP}$*) line. To achieve expression of ChR2 in thalamic afferents, we used a vesicular glutamate transporter

(*VGlut2*, also known as *Slc17a6*) Cre driver mouse line in combination with a ChR2 reporter: *VGlut2*^{Cre};*Rosa26*$^{LSL.ChR2.EYFP}$ or *Olig3*^{Cre};*Rosa26*$^{LSL.ChR2.EYFP}$ (Fig. 1e,f and Supplementary Fig. 4). Re^{+} interneurons were targeted for whole-cell recordings either by using the same electroporation approach we used for monosynaptic rabies or by recording unlabeled layer I cells. In accordance with the anatomical tracing, we recorded light-evoked monosynaptic excitatory responses from these neurons in the presence of tetrodotoxin (TTX) to block polysynaptic events and 4-aminopyridine (4AP) to enhance presynaptic vesicular release[17–19] (Fig. 1e,f and Supplementary Fig. 5). In a separate set of experiments, we further validated these results by recording NMDAR-dependent monosynaptic responses in the presence of AMPA and kainate receptor antagonists (Supplementary Fig. 5b). In these experiments the observed EPSC latencies were around 10 ms, which matched the latencies of the AMPAR-mediated responses in the absence of TTX and 4AP (Supplementary Fig. 5a,c,d). These values are consistent with what has been reported in previous studies using very similar approaches[17–19]. Taken together, the monosynaptic rabies tracing and optogenetic mapping revealed that, during the first postnatal week, developing Re^{+} interneurons positioned in the superficial layers of the cortex receive functional glutamatergic innervation not only from the expected local network, but also from somatosensory thalamic nuclei.

Attenuation of thalamic activity leads to abnormal differentiation of Re^{+} but not VIP^{+} subtypes

Because thalamic afferents provide excitatory drive to Re^{+} interneurons during the first postnatal week (see also Supplementary Fig. 6), we assessed their contribution to the morphological development of these neurons. To manipulate sensory activity relayed through the thalamus, we used a sensory-deprivation protocol[20]. In mice where the Re^{+} population had previously been labeled using *in utero* electroporation with a Dlx5/6-eGFP plasmid, we carried out chronic bilateral whisker plucking during the first postnatal week beginning at birth (Fig. 2a). Thalamic terminals were visualized through their expression of VGlut2 and, in control conditions, were found to typically form barrels in layer IV (Fig. 2b). In contrast, these terminals exhibited an abnormally diffuse termination pattern after sensory deprivation (Fig. 2b). While this manipulation did not perturb cortical layering or interneuron migration (Fig. 2b and Supplementary Fig. 7a,b), analysis of the morphological maturation of Re^{+} interneurons revealed severely truncated axonal arbors and dendritic trees (Fig. 2c,e–g and Supplementary Fig. 7c). This effect was specific to this subtype, as VIP^{+} interneurons, which we have previously shown to be unaffected by other activity manipulations[9], developed proper axo-dendritic arbors in this setting (Fig. 2d,h–j and Supplementary Fig. 7d).

To further characterize the role of thalamic activity, we genetically blocked thalamic transmission and assessed the effect of this manipulation on interneuron maturation. As the *VGlut2*^{Cre} driver also targets some cortical neurons (Supplementary Fig. 4g), we crossed *Olig3*^{Cre} with *Rosa26*$^{LSL.TeLC}$ mice[21], which restricted the expression of the tetanus toxin light chain (TeLC) to thalamic nuclei. The use of the *Rosa26*$^{LSL.TeLC}$ mouse line as an effective method for blockade of synaptic release has been previously documented[22]. Consistent with the expression of the toxin, we found a marked reduction in the levels of

vesicle-associated protein 2 (VAMP2), a synaptic protein cleaved by TeLC and required for synaptic vesicular release (Supplementary Fig. 8). This genetic blockade of thalamic activity led to a more robust disorganization of defined barrels in layer IV as compared to sensory deprivation (Fig. 2b). Furthermore, similarly to those in the whisker-plucked animals, Re^+ interneurons showed morphological impairment after blockade of thalamic glutamate release (Fig. 2c,e–g). These results suggest that thalamic activity is fundamental to the axo-dendritic development of Re^+ interneurons and are consistent with our previous findings indicating that, in contrast to VIP^+ subtypes, Re^+ interneurons are affected by alterations in activity[9].

Severe attenuation of cortical glutamatergic activity does not perturb Re^+ interneuron differentiation

Since the rabies tracing experiments indicated that Re^+ interneurons also receive local cortical inputs, we sought to assess the impact of altering intracortical activity on interneuron development. We began by electroporating $Emx1^{Cre}$ mice with a Dlx5/6-mCherry plasmid at E15.5 to label Re^+ interneurons. Subsequently, we injected an adeno-associated virus (AAV) containing a Cre-dependent genetic switch (FLEx switch) and TeLC.eGFP[23] in the somatosensory and other cortical areas at P1 and analyzed their brains at P8–P10 (Fig. 3a). This experimental strategy has been successfully used to block synaptic output from hippocampal interneurons[23] and cortical neurons[22]. We found that the TeLC.eGFP fusion protein was robustly expressed in pyramidal cells at P8 as reflected by the high levels of eGFP expression (Fig. 3b–d). In an effort to maximize the level of viral expression, we also carried out the viral injections at the time of the electroporation at E15.5. We indeed found that these early injections caused a marked decrease in the VAMP2 protein levels (Fig. 3e). We then reconstructed the morphology of labeled Re^+ interneurons surrounded by pyramidal cells expressing TeLC (Fig. 3f–h) in both sets of experiments and found no significant changes in the length or complexity of axonal arbors and dendritic trees (Fig. 3g,h).

Although we observed a marked decrease in VAMP2 levels upon injection with the AAV-flex-TeLC.eGFP virus (Fig. 3e), we could not formally exclude the possibility that residual cortical glutamatergic signaling to Re^+ interneurons persisted. To achieve a more complete blockade of intracortical glutamate release, we crossed $Emx1^{Cre}$ to $Rosa26^{LSL.TeLC}$ mice. Although the lethality of this cross is high, we obtained a single survivor $Emx1^{Cre};Rosa26^{LSL.TeLC}$ (hereafter, Emx1-TeLC) mouse (out of 15 crosses). It appeared healthy and was undistinguishable from its littermates. Consistent with the cortical expression of tetanus toxin in this mouse, we observed a reduction in VAMP2 levels in the cortex but not in ventral structures (Fig. 3i). To confirm the absence of cortically evoked synaptic responses, we performed *in vitro* electrophysiology and at the same time filled layer I Re^+ interneurons with biocytin to reveal their morphology. In the same session, we recorded from a littermate $Rosa26^{LSL.TeLC}$ (Cre^-) animal. We subsequently recorded from additional $Rosa26^{LSL.TeLC}$ (Cre^-) animals to increase the number of data points for both the electrophysiological and morphological analyses. To test for the blockade of intracortical inputs onto Re^+ interneurons, we placed a bipolar stimulating electrode under the recorded cell in layer II and stimulated at increasing intensities (0.2–3.2 mA) with a 60-μs-long square pulse (Fig. 3j). All control cells displayed evoked EPSCs at −70 mV, but only one of

the cells recorded in the *Emx1-TeLC* animal showed any response, and it was very small, consistent with the reduced levels of VAMP2 protein (*Rosa26*$^{LSL.TeLC}$: −83.89 ± 17.62 pA, n = 14 cells; *Emx1-TeLC*: −3.60 ± 3.60 pA, n = 4 cells; P = 0.0008, Mann-Whitney test) (Fig. 3j,k). Interestingly, though, we were able to evoke EPSCs after placing the stimulating electrode in layer I, presumably by stimulating thalamic afferents, consistent with the specific expression of TeLC in cortical but not thalamic terminals (Fig. 3j,k). Despite the blockade of intracortical excitation, we found that Re^{+} interneurons developed normal morphologies in the *Emx1-TeLC* mouse (Fig. 3l,m).

In an effort to increase the sample size for this analysis, we generated mice containing a *Bhlhb5*^{Cre} allele and *loxP*-flanked (*fl*) *Munc18* (*Stxbp1*) alleles[24]. *Bhlhb5*^{Cre}*;Munc18*$^{fl/fl}$ mice were born at Mendelian frequencies and survived until P15. Despite a marked reduction in cortical thickness (Fig. 3n), Re^{+} interneurons in layer I exhibit normal morphology in *Bhlhb5*^{Cre}*;Munc18*$^{fl/fl}$ mice compared to *Munc18*$^{fl/fl}$ controls (Fig. 3o,p). These results show that we can substantially reduce the afferent intracortical drive to Re^{+} interneurons without noticeably impairing their development. Taken together, our results suggest that early thalamic activity is uniquely critical for the proper morphological development of Re^{+} interneurons. Hence, while it appears likely that, under physiological circumstances, secondary activation of excitatory cortical neurons augments the developmental excitatory drive that neurogliaform cells receive from the thalamus, the direct thalamic excitatory drive to neurogliaform cells alone is sufficient to allow them to develop normally.

Thalamo-cortical inputs preferentially activate NR2B-containing NMDARs

What, then, are the molecular and functional distinctions that result in the differential requirement of thalamic versus intracortical activity for Re^{+} neurogliaform interneuron development? In the hippocampus, inputs from the perforant and Schaffer collateral pathways onto CA1 pyramidal cells can be distinguished by the selective enrichment of NR2B-containing NMDARs[25]. However, whether a similar mechanism could operate in Re^{+} neurogliaform interneurons, which possess smaller dendritic arbors, remained unknown.

NMDAR-mediated currents are prominent in several neuronal populations, including maturing cortical pyramidal cells[26], olfactory granule cells[27] and hippocampal interneurons[28]. To dissect the receptor composition of thalamic and intracortical synapses, we used a *Rosa26*$^{LSL.ChR.EYFP}$ line in combination with either *Emx1*^{Cre} and *Bhlhb5*^{Cre} driver lines, which exclusively target excitatory cortical neurons, or a *VGlut2*^{Cre} driver line, which preferentially (but not exclusively) induces recombination in thalamic neurons (hereafter *Emx1-ChR2* and *VGlut2-ChR2*, respectively) (Fig. 4a and Supplementary Fig. 4). We then performed optogenetic stimulation of the different afferents and recorded NMDAR-dependent responses from Re^{+} interneurons (Fig. 4d–f). Most cortical NMDARs are heterotetramers composed of two obligatory NR1 and two NR2 (NR2A or NR2B) subunits, with hippocampal interneurons expressing both 2A and 2B[28,29]. Notably, depending on the NR2 subunit present, the receptors may display differential downstream signaling pathways[26]. We therefore assessed the NMDAR composition in Re^{+} interneurons activated in *VGlut2-ChR2* and in *Emx1-ChR2* mice, by analyzing their degree of blockade by the

NR2B-specific antagonist ifenprodil. We found that light-evoked NMDAR-mediated synaptic responses showed a larger NR2B-component in *VGlut2-ChR2* than in *Emx1-ChR2* mice (Fig. 4d–f). Based on the observed patterns of ChR2 expression in these two compound genotypes, we infer that the thalamocortical projection preferentially activates NR2B-containing receptors on the Re^+ interneuron population.

In an effort to assess the robustness of the results obtained by our experimental design, we performed two more sets of experiments. First, to activate the intracortical inputs onto Re^+ interneurons, we used a bipolar stimulating electrode placed close to the recorded cell (Supplementary Fig. 9). Second, in an effort to overcome the potentially confounding effect of the cortical expression of VGlut2, we performed thalamic injections with an AAV1.Ef1a.dflox.hChR2.mCherry.WPRE. hGH (where Ef1a represents human elongation factor-1α (*EEF1A*), hChR2 represents an H134R variant and hGH represents the human growth hormone polyadenylation sequence) virus in $VGlut2^{Cre}$ mice at P2 and performed recordings at P9–P12 (Fig. 4b). This strategy allowed robust viral expression in the thalamus without impinging on the cortex (Fig. 4c). Although there was more variability in the AMPA-mediated responses among the thalamically injected mice (possibly due to variability in the levels of ChR2 expression and/or number of thalamic neurons infected with the virus), there was no statistical difference between them and the responses from *VGlut2-ChR2* mice ($P = 0.54$ for charge, Mann-Whitney), and the results we obtained using the two approaches were comparable (Fig. 4 and Supplementary Fig. 9).

Abrogation of NMDAR activity leads to aberrant Re^+ interneuron differentiation

To assess the contribution of NMDARs versus AMPARs to the development of Re^+ interneurons, we carried out genetic and pharmacological blockade of the different types of receptors. To ablate all NMDAR-mediated responses, we co-electroporated Dlx5/6-eGFP and Dlx5/6-Cre plasmids into $NR1^{fl/fl}$ ($Grin1^{fl/fl}$) mice (Fig. 5a). By removing the NR1 subunit, we efficiently ablated NMDAR-dependent currents in $Dlx5/6\text{-}Cre;NR1^{fl/fl}$ Re^+ interneurons while maintaining AMPAR-dependent currents (Fig. 5b). To selectively ablate NR2B-containing receptors, we electroporated $NR2B^{fl/fl}$ mice (Fig. 5a). As judged by comparison of their passive electrophysiological properties and ability to discharge action potentials to control cells, Re^+ interneurons with NMDAR deletion appeared healthy (Supplementary Fig. 10). Re^+ interneurons migrated to their normal position in the somatosensory cortex (data not shown). In both $NR1^{fl/fl}$ and $NR2B^{fl/fl}$ mice, however, we found that, as with manipulations that attenuate thalamocortical output, Re^+ (but not VIP^+) interneurons failed to mature properly and displayed both truncated axonal arbors and dendritic trees (Fig. 5c–h and Supplementary Fig. 10). In a parallel experiment, we observed similar morphological defects after subdural administration of ifenprodil (0.5 nM) at P3 (Supplementary Fig. 11). These defects were specific to the loss of NR2B-containing receptors, as Re^+ interneurons developed normally in $NR2A^{-/-}$ ($Grin2a^{-/-}$) mice (Fig. 6), as well as after blockade of AMPA receptors *in vivo* (Supplementary Fig. 12). Thus, the activation of NR2B-containing NMDARs is selectively required for the proper maturation of Re^+ interneurons allocated to the superficial layers of the cortex.

A critical period for the requirement of NMDARs in morphological development

Our previous observations indicate that activity is required for morphological development of Re^+ interneurons after P3 (ref. 9). To assess whether the requirement for NMDAR activation follows a similar time course, we selectively removed the receptor at different developmental time points. After electroporating Dlx5/6-Cre^{ER} (estrogen receptor) and CAG-STOP-GFP plasmids in *NR1*$^{fl/fl}$ mice at E15.5, we subsequently administered tamoxifen at P3 or P6 and analyzed Re^+ interneuron morphology at P8. Tamoxifen administration at P3 but not at P6 phenocopied the morphological defects observed in the embryonic *Dlx5/6-Cre* ablation experiments (Supplementary Fig. 13). These results indicate that NR2B-containing NMDARs driven by the thalamic inputs are required in Re^+ interneurons between P3 and P6 for their proper morphological development.

Severe reduction of thalamic inputs after abrogation of NMDAR function

Does the morphological impairment observed in NMDAR-ablated Re^+ interneurons preclude their proper integration into nascent cortical circuits? To determine whether the afferent connectivity onto NMDAR-ablated interneurons was affected, we performed monosynaptic rabies tracing after cell-autonomous removal of NMDARs. We first electroporated Dlx5/6-hGFP-TVA-B19G and Dlx5/6-Cre plasmids into *NR1*$^{fl/fl}$ mice and subsequently injected the SADΔG_mCherry(EnvA) virus at P3 (Fig. 7). At P8, we observed a single starter cell (Re^+) per brain in the control (Cre^-, Ctrl; $n = 6$ mice) and the NMDAR-ablated (Cre^+, *Dlx5/6-Cre;NR1*$^{fl/fl}$; $n = 3$ mice) groups, corroborating previous results that ablation of these receptors does not affect Re^+ cell survival. Furthermore, the total number of presynaptic traced cells was not significantly different between control (190 ± 55) and *Dlx5/6-Cre;NR1*$^{fl/fl}$ (150 ± 47; $P = 0.646$) interneurons (Fig. 7d). However, the distribution of presynaptic partners was significantly altered by NMDAR ablation. *Dlx5/6-Cre;NR1*$^{fl/fl}$ interneurons showed a severe reduction in thalamic afferent connectivity (Ctrl: 60% ± 6 versus *Dlx5/6-Cre;NR1*$^{fl/fl}$: 16% ± 2, $P < 0.01$) and a concomitant increase in intracortical pyramidal cell innervation (Ctrl: 14% ± 1 versus *Dlx5/6-Cre;NR1*$^{fl/fl}$: 42% ± 2, $P < 0.0001$) (Fig. 7c,e,f). In contrast, interneuron afferent connectivity was not significantly changed in *Dlx5/6-Cre;NR1*$^{fl/fl}$ interneurons (Ctrl: 27% ± 6 versus *Dlx5/6-Cre;NR1*$^{fl/fl}$: 42% ± 4, $P = 0.103$) (Fig. 7f). It is interesting that, despite developing a rudimentary dendritic tree, *Dlx5/6-Cre;NR1*$^{fl/fl}$ interneurons received exuberant yet aberrant intracortical innervation. Remarkably, even in the presence of substantial glutamatergic signaling through AMPARs, *Dlx5/6-Cre;NR1*$^{fl/fl}$ interneurons failed to develop proper axonal processes and to integrate properly into nascent cortical circuits. Together these data suggest that activation of NMDARs mediates the proper integration of maturing interneurons in the brain.

DISCUSSION

Our results indicate that specific types of early activity play an active and crucial role in directing the formation of selective connectivity patterns. We found that Re^+ neurogliaform interneurons respond differentially to distinct glutamatergic inputs, which regulate their selective synaptic connectivity. Our observations complement recent findings indicating that glutamatergic transmission from retinal ganglion cell (RGC) axons from the ipsilateral eye is fundamental in preventing aberrant contralateral RGC axon innervation in the dorsal

lateral geniculate nucleus (dLGN)[30]. In addition, manipulation of spontaneous cholinergic retinal activity, while sparing overall activity levels, prevents the eye-specific segregation and refinement of RGC projections in the dLGN[31]. Similarly, our activity manipulations affecting NMDAR-mediated signaling, even under conditions that preserve both intrinsic electrophysiological properties and AMPAR-mediated responses, resulted in profound neuronal maturation defects.

Re^+ interneurons in the somatosensory cortex receive abundant local innervation from pyramidal cells, as revealed by glutamate uncaging in adult cortical slices[12]. In addition to this pattern of local connectivity, recent experimental evidence has revealed that Re^+ interneurons of layer I in the prefrontal cortex receive monosynaptic connections from the thalamic ventromedial nucleus and in turn provide feedforward inhibition to layer II pyramidal cells[17]. Together these findings suggest that the appropriate connectivity of Re^+ interneurons (and perhaps other subtypes) may depend on critical specific interactions occurring when interneurons cease migrating and attain their final position. Our *in vivo* analysis provides one example in which Re^+ interneurons allocated to layers I through III receive strong thalamic drive during development, which is essential in determining their mature connectivity.

In addition to providing specific insights regarding the development of connectivity onto Re^+ interneurons, our findings suggest that monosynaptic tracing using the rabies virus provides an effective method for determining the afferent connectivity of cortical neurons at different developmental time points. Furthermore, to rule out a bias of the rabies tracing to GABAergic and glutamatergic synapses, we carried out the same experiment in a larger subset of superficial interneurons, including VIP- and calretinin-expressing subtypes. We found that, in contrast to Re^+ interneurons, these populations of superficial interneurons received innervation from the nucleus basalis at P6, indicating that the rabies tracing strategy does not preclude *per se* the tracing of these synapses (Supplementary Fig. 3). These results are in agreement with recently published data on rabies tracing of mature VIP^+ interneurons[32]. VIP^+ interneurons present in the visual cortex receive substantial innervation from intracortical populations and the nucleus basalis, with a minor contribution from the dLGN, indicating that the rabies virus does not preferentially label thalamic synapses over cortical or cholinergic ones.

Our findings extend previous work demonstrating that sensory experience shapes the topography of the sensory cortices[33–37] directly and not through second order cortical neurons. To exclude generalized effects of activity on cortical cytoarchitecture, we performed a more restricted manipulation of thalamic activity, whisker-plucking, which does not cause layering defects, and confined our analysis to the first postnatal week. Indeed, the total number and the distribution of pyramidal cells in superficial and deep layers were similar in control and sensory-deprived brains (Fig. 2b and Supplementary Fig. 7a,b). Similar results were obtained after genetic blockade of thalamic transmission (Fig. 2b–g and Supplementary Fig. 8). In spite of the normal layering of the cortex at P8, these manipulations induced profound defects in the morphological development of Re^+ interneurons.

How do different afferent sources of excitation differentially impact development? Re^+ interneurons distinguished between seemingly similar inputs on the basis of the postsynaptic receptors that the afferents impinge on. The prominent requirement for NMDARs during CNS maturation is well established[26]. In cortical excitatory neurons, the NR2B subunit is required for proper dendritic patterning[38] and is also differentially used by hippocampal interneuron subtypes sharing the same embryonic origin as the Re^+ interneurons studied here[28]. Our results extend these observations and suggest that there is a preferential allocation of NR2B-containing NMDARs to the postsynaptic sites in the dendrites of Re^+ interneurons that receive thalamic input.

The present results, combined with findings from both our laboratory[9] and others[39], suggest that the roles of activity in interneuron development are both specific to subtype and multifaceted, and affect both migration and differentiation. Re^+ but not VIP^+ interneurons failed to migrate to appropriate laminae and displayed impaired morphological maturation after an overall dampening of neuronal excitability. Similarly, Re^+ but not VIP^+ interneurons failed to develop normal axonal arbors and dendritic trees after sensory deprivation, genetic blockade of thalamic glutamate release or blockade of NMDAR-dependent currents. These results indicate that Re^+ neurogliaform interneurons are critically reliant on electrical activity to mature and integrate into cortical circuits, whereas VIP^+ interneurons may use either intrinsic genetic programs or as-yet-unidentified sources of activity. Thus, an intriguing combination of intrinsic and extrinsic mechanisms is used for the integration of distinct interneurons into cortical circuits.

In summary, our results indicate that emergent electrical activity is crucial in shaping the assembly of select cortical neuronal circuits. These observations emphasize that understanding how brain wiring is achieved will require a case-by-case examination of how different cell types and the cortical microcircuits they contribute to are assembled. This in turn suggests that developmental insults are likely to differentially affect the formation of specific circuit configurations. As such, understanding the rules governing the integration of different interneurons subtypes into cortical circuits may provide insights into the pathogenesis of neuropsychiatric disease.

METHODS

Methods and any associated references are available in the online version of the paper.

ONLINE METHODS

Mouse strains

Pregnant mice were electroporated at 15 d of gestation (E15.5). Strains from Jackson laboratories used in this study include Swiss Webster, $NR1^{fl}$, $Emx1^{Cre}$, $VGlut2^{Cre}$, RCE^{fl} and $Ros26^{LSL.ChR2.EYFP}$ (*Ai32*). In addition, we used $Olig3^{Cre}$ (a gift from Y. Nakagawa, University of Minnesota), $Bhlhb5^{Cre}$ (a gift from L. Gan, University of Rochester Medical Center), $R26^{floxstop\text{-}TeNT}$ (which we called $Rosa26^{LSL.TeLC}$ for consistency with the viral tools; a gift from M. Goulding, Salk Institute for Biological Studies), $NR2A^{-/-}$ (a gift from S. Nakanishi, Kyoto University), $NR2B^{fl}$ (a gift from H. Monyer, University of Heidelberg),

a *Munc18*$^{fl/fl}$ (a gift from M. Verhage, VU University Amsterdam) and a *5HT3A*^{Cre} (a gift from N. Henitz, Rockefeller University) mouse lines. Tamoxifen (20 mg/ml in corn oil; 50–100 µl per pup) was administered by oral gavage at selected time points (P3, P6). Information about the mouse strains including genotyping protocols can be found at http://www.jax.org/ and elsewhere[21,24,27,40,41].

In utero electroporation

The protocol for mouse *in utero* electroporation has been described elsewhere[9,42,43]. The plasmids used in the electroporation experiments were generated using standard cloning techniques. To generate the Dlx5/6-hGFP-TVA-B19G plasmid, the H2BGFP-F2A-TVA-T2A-B19 fragment (a gift from M. Goulding, Salk Institute for Biological Studies) was cloned into a Dlx5/6-Pmin-polyA plasmid. Mouse colony maintenance and handling was performed in compliance with the protocols approved by the Institutional Animal Care and Use Committee of the New York University School of Medicine.

Viral injections

Adeno-associated virus containing the eGFP-tagged tetanus toxin light chain (TeLC) reading frame inverted in a Flip-excision (flex) cassette[23] (AAV1/2.flex.TeLC.eGFP) (a gift from P. Wulff, University of Aberdeen) was injected unilaterally into the cortex of electroporated (Dlx5/6.mCherry) wild-type mice at E15.5 or P0. For the E15.5 viral injections, we first performed the electroporation and promptly injected the AAV virus in the developing cortex of *Emx1*^{Cre} embryos. For all postnatal injections, animals were anesthetized by inducing hypothermia on ice and kept on either ice wrapped in a cloth or an ice-cold clay mold. For rabies tracing experiments, recombinant mCherry-expressing, ASLV-A envelope glycoprotein (EnvA)-pseudotyped, glycoprotein-deleted rabies virus SADG-mCherry(EnvA) (gift from E. Callaway, Salk Institute for Biological Studies)[44,45] was injected unilaterally into the cortex of electroporated wild-type, *NR1*$^{fl/fl}$ or *5HT3A*^{Cre} mice between postnatal days 0 and 3. To achieve ChR2 expression in thalamic terminals, we unilaterally and stereotactically injected AAV1.Ef1a.dflox.hChR2.mCherry.WPRE.hGH (University of Pennsylvania viral vector core) into the thalamus of *VGlut2*^{Cre} animals at P2. In these experiments, we did not observe any ectopic expression of the virus in the neocortex, as judged by immunofluorescence and the lack of light-induced depolarization in randomly picked excitatory cells around the injection site. For the rabies experiments, we injected 100 nl of virus; for the thalamic ones, 300 nl. These injections were done over a 2-min period using a glass micropipette (tip diameter ~20 µm) attached to a Nanolitre 2000 pressure injection apparatus (World Precision Instruments). The pipette was held in place for 2 min after each injection before being completely retracted from the brain. To allow for adequate virus expression after the injection, mice were returned to their home cage for 5–9 d before either fixing the brain for cryostat section analysis or using a vibratome for acute slice preparation and electrophysiology.

Immunohistochemistry, neuronal morphology analysis and subdural injections

The methodology for these analyses has been previously described[9]. The identity of presynaptic partners identified by means of rabies monosynaptic tracing was determined by

coexpression of mCherry (SADG-mCherry(EnvA)), excitatory cell markers (rabbit anti-RORβ, 1:1000 (a gift from G. Miyoshi, New York School of Medicine); rabbit anti-CTIP2, 1:1000, Abcam (ab28448); rabbit anti-Tbr1, 1:1000, Abcam (ab31940); rabbit anti-Satb2, 1:500, Abcam (3ab4735) and GABAergic interneuron markers (guinea pig anti-GABA, Abcam (ab17413), mouse anti-Reelin, 1:500, MBL (D223-3); rabbit anti-dsRED, Abcam (ab62341)). For assessing the effectiveness of tetanus toxin expression, we used a mouse anti-VAMP2 BT antibody (1:200, Synaptic Systems 104 211BT). Successful targeting of the desired Re^+ and VIP^+ populations in all of our experiments was confirmed through *post hoc* examination of marker expression (rabbit anti-VIP 1:1000, Immunostar, 20077). The morphology of Cre^+ $NR1^{fl/+}$ and $NR2B^{fl/+}$ interneurons was not significantly different than that of control Cre^- $NR1^{fl/fl}$ or $NR2B^{fl/fl}$ interneurons (*Cre-NR1*$^{fl/fl}$ versus *Cre-NR2B*$^{fl/fl}$: axonal length, $P = 0.30$; dendritic length, $P = 0.11$); therefore, these interneurons were all grouped in the controls. Similarly, wild-type non-sensory-deprived and $Rosa26^{LSL.TeLC}$ mice were grouped in the control group (axonal length, $P = 0.222$; axonal nodes, $P = 0.793$; dendritic length, $P = 0.879$). Finally, $NR2A^{+/+}$ and $NR2A^{+/-}$ mice were also grouped in a control group (axonal length, $P = 0.33$; axonal nodes, $P = 0.73$; dendritic length, $P = 0.563$; dendritic nodes, $P = 1$).

Analysis of presynaptic inputs

To quantify the number of cortical and subcortical inputs, all cryostat sections from an individual rabies-infected brain were collected for analysis. Confocal *z*-stacks were analyzed with the custom-made Matlab plug-in “Reference Axes”[13]. The program allowed digitalization of the images and quantification of cortical excitatory ($Tbr1^+$, $Ctip2^+$, $ROR\beta^+$, $Satb2^+$) neurons, thalamic (VPM and POm) and GABAergic interneurons ($GABA^+$). Morphological criteria were also used to confirm the identity of the neurons. The identity of presynaptic inputs was determined as the proportion of the total number of $mCherry^+$ neurons (cortical and thalamic) that expressed either cortical excitatory or GABAergic markers or were located in the VPM and POm nuclei of the thalamus. For identification of the starter cells in the rabies tracing experiments, 20-μm cryostat sections were analyzed for GFP and mCherry coexpression under an Olympus upright microscope equipped for multi-fluorescence analysis before processing the tissue for immunohistochemistry. The sections that showed cells coexpressing GFP and mCherry (starter cells) were processed for immunohistochemistry against Reelin, GFP and mCherry. All of the brains used in our experiments exhibited a single Re^+ starter cell (Supplementary Fig. 2). The sections that did not contain starter cells (240–280 sections per brain) were processed for presynaptic partner analysis. Immunohistochemistry was performed on these sections with a cocktail of rabbit antibodies against excitatory cell markers (Satb2, Ctip2, RORβ, Tbr1) and a guinea pig anti-GABA antibody to label interneurons. Subsequently, the sections were processed with anti-rabbit Alexa 488 and anti–guinea pig Cy5 secondaries in combination with mCherry fluorescence to identify $mCherry^+$ cortical excitatory and inhibitory neurons.

Electrophysiology and analysis

Whole-cell patch-clamp electrophysiological recordings were performed on eGFP-positive and eGFP-negative cells of layers I–III in acute brain slices prepared from P8–P12 animals. No data reported have been previously published with the exception of the control and

Kir2.1-expressing Re^+ cells used for comparison of the intrinsic electrophysiological properties to the NMDA receptor knockout Re^+ cells[42] (Supplementary Fig. 10).

Briefly, animals were decapitated and the brain was dissected out and transferred to physiological Ringer's solution (ACSF) cooled to 4 °C, of the following composition (mM): 125 NaCl, 2.5 KCl, 25 $NaHCO_3$, 1.25 NaH_2PO_4, 1 $MgCl_2$, 2 $CaCl_2$ and 20 glucose. The brain was then glued to a stage and slices 250–300 μm were cut using a vibratome (Vibratome 3000 EP). The slices were allowed to recover in recording ACSF at room temperature for at least 45 min before recording. Acute slices were then placed in a recording chamber mounted on the stage of an upright microscope (Axioscope, Zeiss, Germany) equipped with immersion differential interference contrast objectives (5×, 40×) coupled to an infrared camera system (Zeiss), superfused at a rate of 1–2 ml/min with oxygenated recording ACSF and maintained at a temperature of 31 °C. An EGFP filter was used to visualize the fluorescent interneurons in epifluorescence.

Patch electrodes were made from borosilicate glass (Harvard Apparatus) and had a resistance of 4–8 MΩ. For both intrinsic electrophysiological properties and spontaneous excitatory postsynaptic current (sEPSC) recordings, the patch pipettes were filled with a solution containing the following (in mM): 128 potassium gluconate, 4 NaCl, 0.3 Na-GTP, 5 Mg-ATP, 0.0001 $CaCl_2$, 10 HEPES.

For acquisition of both AMPA receptor–mediated and NMDA receptor–mediated excitatory currents in the same cell, the pipettes were filled with the following (in mM): 126 cesium methanesulfonate, 4 CsCl, 0.3 Na-GTP, 4 Mg-ATP, 10 HEPES, 20 D-trisphosphocreatine. In all cases 5 mg/ml biocytin (Sigma) was added in the recording solutions.

All experiments that involved extracellular stimulation with an electrode or optogenetic stimulation of channel rhodopsin were performed in voltage clamp in the presence of $GABA_A$ receptor blockers, either bicuculine (20 μM) or SR95531 (20 μM), except for slices from the $Emx1^{Cre};Rosa26^{LSL.TeLC/TeLC}$ animal, where no drugs were added. AMPAR-mediated currents were recorded at −70 mV, whereas NMDAR-mediated currents were recorded at +40 mV in the presence of 20 μM CNQX. For all optogenetic stimulation experiments, TTX (1 μM) and 4-aminopyridine (400–800 μM) were present in the bath unless otherwise specified.

The blue light source (Mightex BioLED Light Source, 470 nm or Polygon 400) used to stimulate channel rhodopsin was mounted on the microscope either in place of the binoculars or on the side between the camera and the objective, in which case light was directed toward the specimen by means of a dichroic mirror. In both cases, light reached the slice through a 40× Zeiss objective. The light intensity used with the BioLED in the presence of TTX and 4AP was 100% and the duration was set to obtain the optimal monosynaptic responses (50–100 ms long). When using the Polygon 400 to stimulate thalamic fibers expressing Ch2R via AAV injections in the presence of TTX and 4AP, the duration and intensity used was more variable: 5–50 ms and 5–100%, respectively. The inter-stimulus interval was always set to 15–20 s to allow for a full recovery of the activated channels.

Experiments were performed in current-clamp and voltage-clamp modes using the Axopatch 200B amplifier (Molecular Devices). sEPSCs were recorded in multiple epochs of 2–4 min at V_h = −70 mV with a sampling rate of 10 kHz and were filtered online at 3 kHz. The recorded sEPSCs were analyzed using Minianalysis software (Synaptosoft, Decatur, GA, USA) or Clampfit. The evoked synaptic values were obtained from the average trace after visual inspection of individual events. The area was measured as an absolute value of the integral of the synaptic current. The latency was measured as the time between the beginning of the deflection of the electrical stimulus artifact or the light onset and the onset of the synaptic current. The decay time was calculated by fitting the average trace with a single exponential. When performing extracellular stimulation, a rate of 0.1 Hz was delivered by using rectangular pulses of 0.05–0.1 ms width with a concentric platinum/iridium bipolar electrode (CBARC75, FHC, Brunswick, ME) connected to a constant-current isolation unit (Digitimer LTD, Model DS3). The intensity of stimulation was usually 1.5–2.5 times the minimum intensity required to evoke a response. This intensity evoked a single synaptic component most of the time. The stimulation electrode was placed at the bottom right side of the recorded cell in layer 2 and right next to the cell when moved to layer 1. Access resistance was always monitored to ensure the stability of recording conditions. Cells were accepted for analysis only if the initial series resistance was less than or equal to 40 MΩ and did not change by more than 20% throughout the recording period. No compensation was made for access resistance and no correction was made for the junction potential between the pipette and the ACSF.

Passive and active membrane properties were recorded in current-clamp mode by applying a series of sub- and suprathreshold current steps. The analysis was done in Clampfit. The resting membrane potential was ascertained in current clamp right after rupturing the patch by applying zero current. All values presented in the manuscript are average ± s.e.m. and all comparisons have been done using a Mann-Whitney test.

The data from the *Bhlhb5*^{Cre} × *Ai32* and *Emx1*^{Cre} × *Ai32* crosses were collected from 4 cells from the *Bhlhb5*^{Cre} × *Ai32* cross and 7 cells from the *Emx1Cre* × *Ai32* cross. We compared to the two data sets for the NMDA/AMPA charge ratio, percentage of amplitude and percentage charge reduction by ifenprodil. The *P* values are, for NMDA/AMPA charge ratio, $P = 0.894$; for percentage of NMDA amplitude reduction, $P = 0.567$; for percentage of NMDA charge reduction, $P = 0.833$). On the basis of these data, we grouped the values from the two crosses together and compared them to the ones we got from the *VGlut*^{Cre} × *Ai32* cross and the *VGlut2*^{Cre} thalamic injection at P2.

Whisker trimming protocol and morphological analysis

Previously electroporated (*Dlx5/6-eGFP*) newborn pups were subjected to whisker plucking daily from P0 to P8. Pups from the same litter were randomly divided into two groups. In the experimental group, all the whiskers and most of the facial hair on the whisker pad were plucked bilaterally using sterile forceps, whereas in the control group all the whiskers were spared. During the procedure, all pups from both groups were briefly separated from the dam and anesthetized by inducing hypothermia (3–5 min) and subsequently allowed to recover on a heating pad after completion of the procedure and returned to their dam. We

analyzed the morphology of control (n = 24), sensory-deprived (n = 12) and TeLC (n = 8) interneurons.

Statistical analysis

Statistical analysis was performed by using either unpaired t-tests (two-tailed distribution) or Mann-Whitney U tests. For all electrophysiology data analysis, the nonparametric Mann-Whitney test was chosen, as the number of values compared was not high enough to merit a normality test and usage of the unpaired t-test. All values represent mean values ± s.e.m. For all other data, normality and equality of variance were formally tested with SPSS Statistics software. The experiments were not blinded to genotype. No statistical methods were used to predetermine sample sizes, but our sample sizes are similar to those reported in previous publications[9,42].

A **Supplementary Methods Checklist** is available.

Supplementary Material

Refer to Web version on PubMed Central for supplementary material.

Acknowledgments

We are grateful to S. Arber, B. Benedetti, J. Burrone, X. Jaglin, J. Kaltschmidt, S. Lee, D. Pisapia and S. Shi for comments on the manuscript. We thank E. Callaway (Salk Institute for Biological Sciences) for providing the recombinant rabies virus; M. Tripodi, A. Ponti and S. Arber for guidance with the rabies method analysis; and L. Yin, J. Deng and J. Dai for technical assistance. N.V.D.M.G. is a recipient of a NARSAD Young Investigator Award and is also supported by grants from the US National Institutes of Health (5 K99 MH095825-02; 3 K99 MH095825-02S1). T.K. has been supported by the Patterson Trust postdoctoral fellowship in brain circuitry and a Roche postdoctoral fellowship. Research in the Fishell laboratory is supported by the US National Institutes of Health, National Institute of Mental Health, National Institute of Neurological Disorders and Stroke, New York State Stem Cell Science and the Simons Foundation.

References

1. Lien AD, Scanziani M. Tuned thalamic excitation is amplified by visual cortical circuits. Nat Neurosci. 2013; 16:1315–1323. [PubMed: 23933748]
2. Ma T, et al. Subcortical origins of human and monkey neocortical interneurons. Nat Neurosci. 2013; 16:1588–1597. [PubMed: 24097041]
3. Hansen DV, et al. Non-epithelial stem cells and cortical interneuron production in the human ganglionic eminences. Nat Neurosci. 2013; 16:1576–1587. [PubMed: 24097039]
4. Pfeffer CK, Xue M, He M, Huang ZJ, Scanziani M. Inhibition of inhibition in visual cortex: the logic of connections between molecularly distinct interneurons. Nat Neurosci. 2013; 16:1068–1076. [PubMed: 23817549]
5. Pi HJ, et al. Cortical interneurons that specialize in disinhibitory control. Nature. 2013; 503:521–524. [PubMed: 24097352]
6. Lee S, Kruglikov I, Huang ZJ, Fishell G, Rudy B. A disinhibitory circuit mediates motor integration in the somatosensory cortex. Nat Neurosci. 2013; 16:1662–1670. [PubMed: 24097044]
7. Palmer LM, et al. The cellular basis of $GABA_B$-mediated interhemispheric inhibition. Science. 2012; 335:989–993. [PubMed: 22363012]
8. Letzkus JJ, et al. A disinhibitory microcircuit for associative fear learning in the auditory cortex. Nature. 2011; 480:331–335. [PubMed: 22158104]
9. De Marco García NV, Karayannis T, Fishell G. Neuronal activity is required for the development of specific cortical interneuron subtypes. Nature. 2011; 472:351–355. [PubMed: 21460837]

10. Wickersham IR, Finke S, Conzelmann KK, Callaway EM. Retrograde neuronal tracing with a deletion-mutant rabies virus. Nat Methods. 2007; 4:47–49. [PubMed: 17179932]
11. Petersen CC. The functional organization of the barrel cortex. Neuron. 2007; 56:339–355. [PubMed: 17964250]
12. Xu X, Callaway EM. Laminar specificity of functional input to distinct types of inhibitory cortical neurons. J Neurosci. 2009; 29:70–85. [PubMed: 19129386]
13. Tripodi M, Stepien AE, Arber S. Motor antagonism exposed by spatial segregation and timing of neurogenesis. Nature. 2011; 479:61–66. [PubMed: 22012263]
14. Miyamichi K, et al. Cortical representations of olfactory input by trans-synaptic tracing. Nature. 2011; 472:191–196. [PubMed: 21179085]
15. Fishell G, Rudy B. Mechanisms of inhibition within the telencephalon: “where the wild things are. Annu Rev Neurosci. 2011; 34:535–567. [PubMed: 21469958]
16. Lee S, Hjerling-Leffler J, Zagha E, Fishell G, Rudy B. The largest group of superficial neocortical GABAergic interneurons expresses ionotropic serotonin receptors. J Neurosci. 2010; 30:16796–16808. [PubMed: 21159951]
17. Cruikshank SJ, et al. Thalamic control of layer 1 circuits in prefrontal cortex. J Neurosci. 2012; 32:17813–17823. [PubMed: 23223300]
18. Petreanu L, Mao T, Sternson SM, Svoboda K. The subcellular organization of neocortical excitatory connections. Nature. 2009; 457:1142–1145. [PubMed: 19151697]
19. Mao T, et al. Long-range neuronal circuits underlying the interaction between sensory and motor cortex. Neuron. 2011; 72:111–123. [PubMed: 21982373]
20. Toda T, et al. Birth regulates the initiation of sensory map formation through serotonin signaling. Dev Cell. 2013; 27:32–46. [PubMed: 24135230]
21. Zhang Y, et al. V3 spinal neurons establish a robust and balanced locomotor rhythm during walking. Neuron. 2008; 60:84–96. [PubMed: 18940590]
22. Xu W, Sudhof TC. A neural circuit for memory specificity and generalization. Science. 2013; 339:1290–1295. [PubMed: 23493706]
23. Murray AJ, et al. Parvalbumin-positive CA1 interneurons are required for spatial working but not for reference memory. Nat Neurosci. 2011; 14:297–299. [PubMed: 21278730]
24. Dudok JJ, Groffen AJ, Toonen RF, Verhage M. Deletion of Munc18–1 in 5-HT neurons results in rapid degeneration of the 5-HT system and early postnatal lethality. PLoS ONE. 2011; 6:e28137. [PubMed: 22140524]
25. Arrigoni E, Greene RW. Schaffer collateral and perforant path inputs activate different subtypes of NMDA receptors on the same CA1 pyramidal cell. Br J Pharmacol. 2004; 142:317–322. [PubMed: 15155538]
26. Wang CC, et al. A critical role for GluN2B-containing NMDA receptors in cortical development and function. Neuron. 2011; 72:789–805. [PubMed: 22153375]
27. Kelsch W, Li Z, Eliava M, Goengrich C, Monyer H. GluN2B-containing NMDA receptors promote wiring of adult-born neurons into olfactory bulb circuits. J Neurosci. 2012; 32:12603–12611. [PubMed: 22956849]
28. Matta JA, et al. Developmental origin dictates interneuron AMPA and NMDA receptor subunit composition and plasticity. Nat Neurosci. 2013; 16:1032–1041. [PubMed: 23852113]
29. Sanz-Clemente A, Nicoll RA, Roche KW. Diversity in NMDA receptor composition: many regulators, many consequences. Neuroscientist. 2013; 19:62–75. [PubMed: 22343826]
30. Koch SM, et al. Pathway-specific genetic attenuation of glutamate release alters select features of competition-based visual circuit refinement. Neuron. 2011; 71:235–242. [PubMed: 21791283]
31. Xu HP, et al. An instructive role for patterned spontaneous retinal activity in mouse visual map development. Neuron. 2011; 70:1115–1127. [PubMed: 21689598]
32. Fu Y, et al. A cortical circuit for gain control by behavioral state. Cell. 2014; 156:1139–1152. [PubMed: 24630718]
33. Morishita H, Hensch TK. Critical period revisited: impact on vision. Curr Opin Neurobiol. 2008; 18:101–107. [PubMed: 18534841]

34. Li H, et al. Laminar and columnar development of barrel cortex relies on thalamocortical neurotransmission. Neuron. 2013; 79:970–986. [PubMed: 24012009]
35. Katz LC, Shatz CJ. Synaptic activity and the construction of cortical circuits. Science. 1996; 274:1133–1138. [PubMed: 8895456]
36. Li H, Crair MC. How do barrels form in somatosensory cortex? Ann NY Acad Sci. 2011; 1225:119–129. [PubMed: 21534999]
37. Dunn FA, Della Santina L, Parker ED, Wong RO. Sensory experience shapes the development of the visual system's first synapse. Neuron. 2013; 80:1159–1166. [PubMed: 24314727]
38. Espinosa JS, Wheeler DG, Tsien RW, Luo L. Uncoupling dendrite growth and patterning: single-cell knockout analysis of NMDA receptor 2B. Neuron. 2009; 62:205–217. [PubMed: 19409266]
39. Bortone D, Polleux F. KCC2 expression promotes the termination of cortical interneuron migration in a voltage-sensitive calcium-dependent manner. Neuron. 2009; 62:53–71. [PubMed: 19376067]
40. Vue TY, et al. Thalamic control of neocortical area formation in mice. J Neurosci. 2013; 33:8442–8453. [PubMed: 23658181]
41. Joshi PS, et al. Bhlhb5 regulates the postmitotic acquisition of area identities in layers II–V of the developing neocortex. Neuron. 2008; 60:258–272. [PubMed: 18957218]
42. Karayannis T, De Marco Garcia NV, Fishell GJ. Functional adaptation of cortical interneurons to attenuated activity is subtype-specific. Front Neural Circuits. 2012; 6:66. [PubMed: 23015781]
43. De Marco Garcia NV, Fishell G. Subtype-selective electroporation of cortical interneurons. J Vis Exp. 2014:e51518. [PubMed: 25177832]
44. Miyamichi K, Luo L. Neuroscience. Brain wiring by presorting axons. Science. 2009; 325:544–545. [PubMed: 19644096]
45. Wickersham IR, et al. Monosynaptic restriction of transsynaptic tracing from single, genetically targeted neurons. Neuron. 2007; 53:639–647. [PubMed: 17329205]

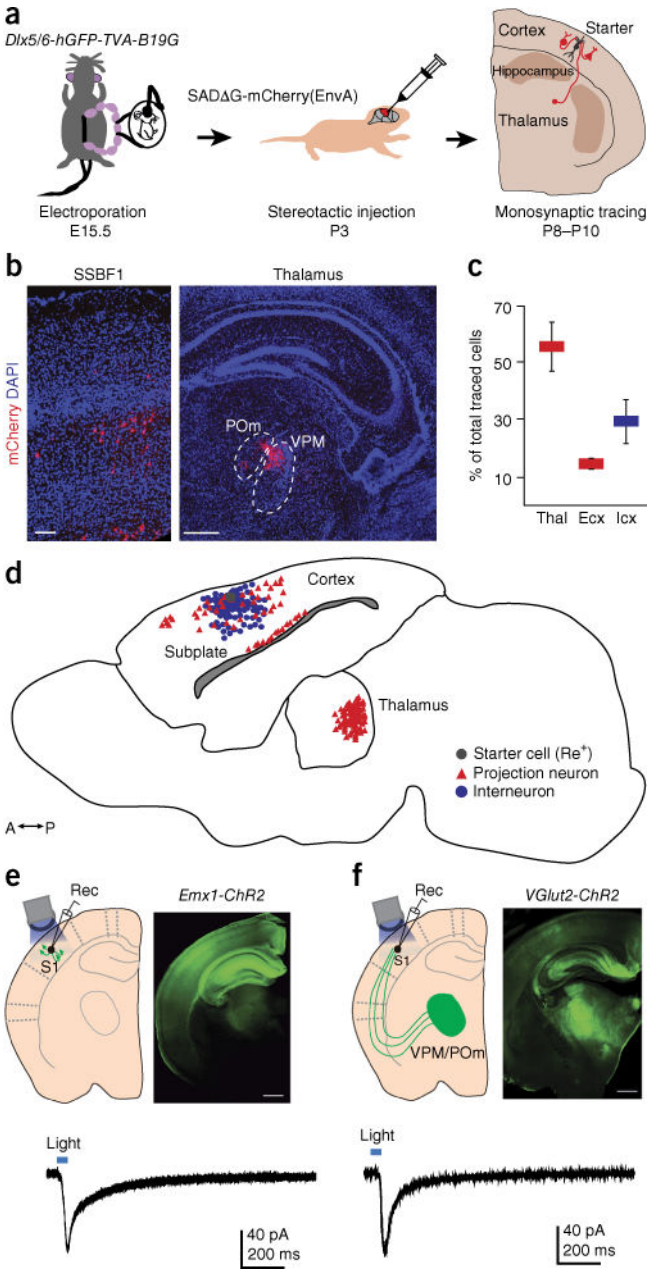

Figure 1.

Determining the afferent inputs onto developing Re^+ interneurons in layers I/III. (**a**) Schematic representation of the experimental strategy. (**b**) Presynaptic partners to a single starter Re^+ interneuron in the somatosensory (SSBF1) cortex and thalamus (see also Supplementary Fig. 2). (**c**) Quantification of the identity of presynaptic inputs. Mean values (±s.e.m.) were obtained from 5 mice. (**d**) The pattern of presynaptic connectivity revealed by rabies tracing to a single Re^+ interneuron in a wild-type P8 mouse brain. (**e,f**) Recording of AMPAR-mediated monosynaptic responses from Re^+ interneurons after *in vitro* light stimulation in $Emx1^{Cre}$; $Rosa26^{LSL\text{-}ChR2\text{-}EYFP}$ (*Emx1-ChR2*) (**e**) and $VGlut2^{Cre}$;$Rosa26^{LSL\text{-}ChR2\text{-}EYFP}$ (*VGlut2-ChR2*) (**f**) mice. Thal, thalamic neurons; Ecx,

cortical excitatory neurons; Icx, cortical interneurons. Scale bars in **b**, 50 μm (SSBF1) and 500 μm (thalamus); in **e** and **f**, 500 μm.

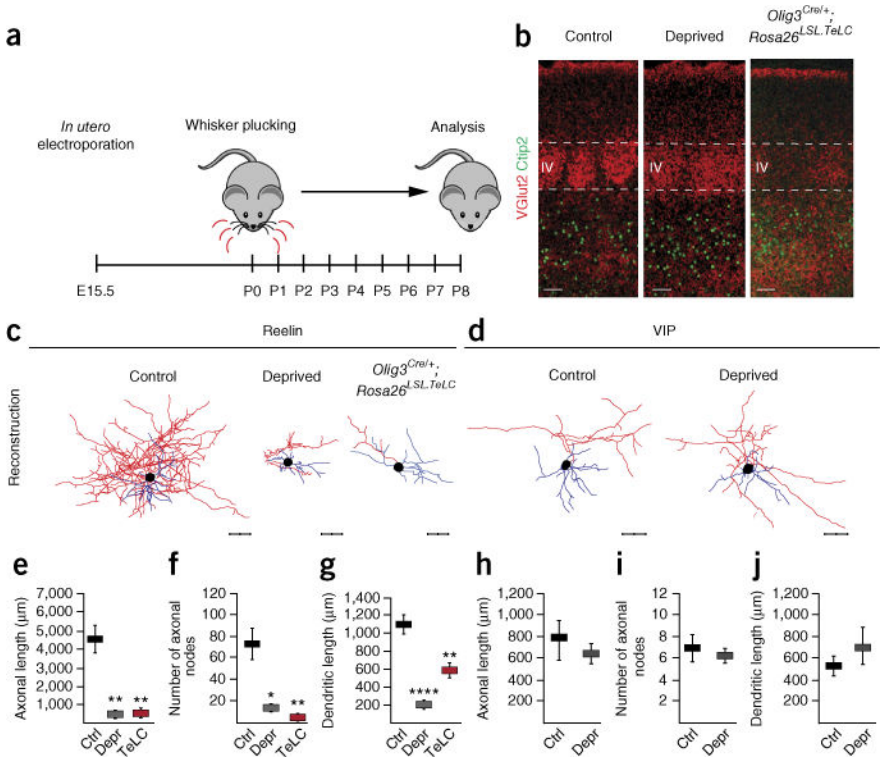

Figure 2.

Perturbation of sensory inputs during the first postnatal week disrupts the axo-dendritic development of Re^+ interneurons. (**a**) Protocol for sensory deprivation. (**b**) Normal layering but diffuse barrel boundaries are observed in the somatosensory cortex of sensory-deprived and *Olig3*$^{Cre/+}$; *Rosa26*$^{LSL.TeLC}$ mice. Control: wild-type, non-sensory-deprived *Rosa26*$^{LSL.TeLC}$ mice. (**c**) Severe morphological defects are present in Re^+ interneurons after whisker plucking and in *Olig3*$^{Cre/+}$;*Rosa26*$^{LSL.TeLC}$ (TeLC) mice. (**d**) Representative examples of neurolucida reconstructions of VIP^+ interneurons in control and sensory-deprived mice. (**e–g**) Quantification of neurite defects. Mean values (±s.e.m.) were obtained from reconstructed Re^+ interneurons each in Dlx5/6-eGFP–electroporated control (Ctrl, n = 7 interneurons), sensory-deprived (Depr, n = 5 interneurons; Ctrl versus Depr: axonal length, P = 0.004; axonal nodes, P = 0.011; dendritic length, P = 0.00006) and TeLC mice (n = 6 interneurons; Ctrl versus TeLC: axonal length, P = 0.003; axonal nodes, P = 0.005; dendritic length, P = 0.004). (**h–j**) Quantification of length and complexity of dendritic tree and axonal arbors of VIP^+ interneurons (mean values ±s.e.m.; Ctrl n = 12 interneurons; Depr n = 4 interneurons; axonal length, P = 0.335; axonal nodes, P = 0.273; dendritic length, P = 0.685). *P < 0.05; **P < 0.01; ***P < 0.001, ****P < 0.0001. Unpaired t-test. Scale bars for **b–d**, 50 µm. Axons are shown in red, dendrites in blue.

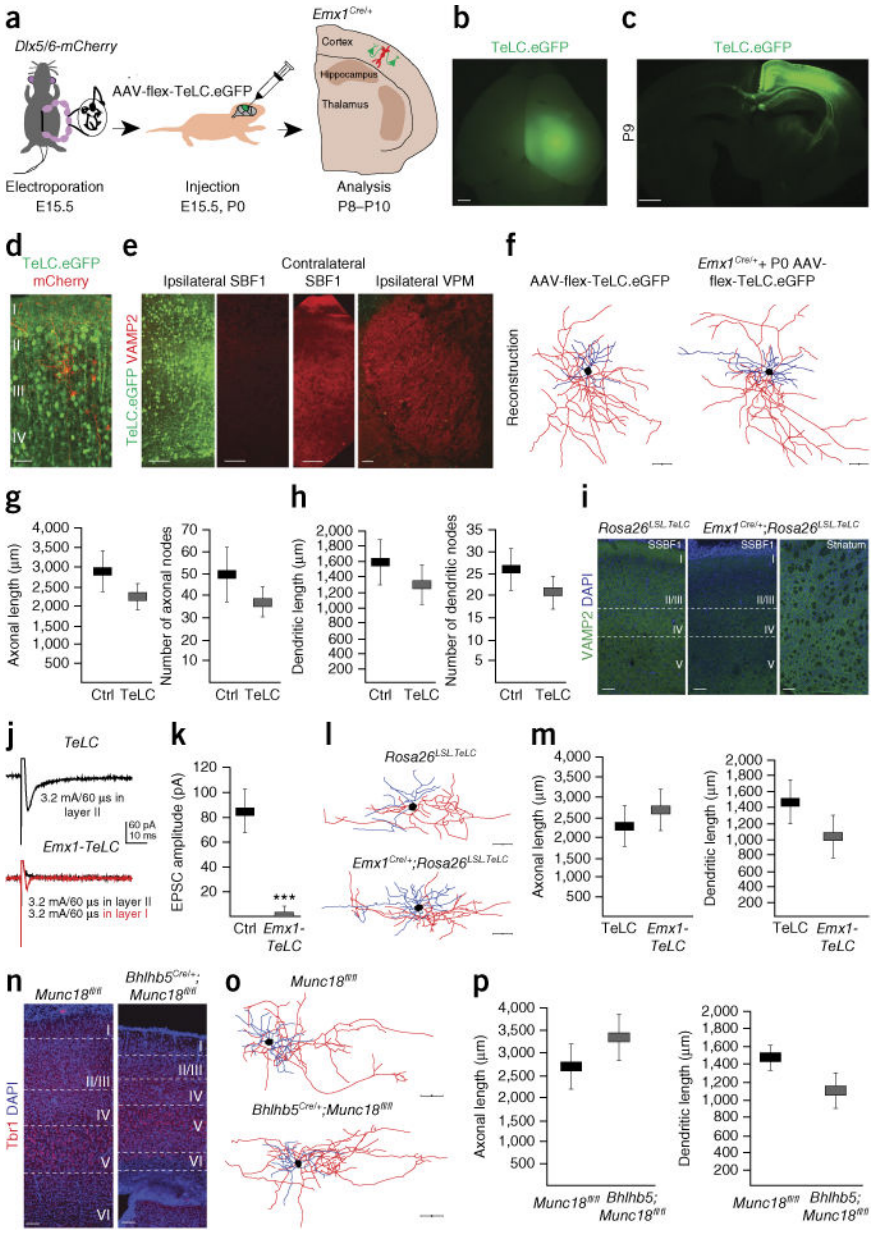

Figure 3.

Severe attenuation of intracortical glutamate release does not interfere with Re^{+} interneuron morphological development. (**a**) Schematic representation of the experimental strategy. (**b**) Whole-mount epifluorescence image showing cortical expression of TeLC.eGFP surrounding the injection site in an *Emx1*$^{Cre/+}$ mouse. (**c**) Coronal section at P9 at the level of the injection site in SSBF1 shows that eGFP expression is restricted to cortical neurons. (**d**) Electroporated interneurons (mCherry^{+}) are surrounded by pyramidal cells expressing TeLC.eGFP (green). (**e**) Reduced levels of VAMP2 protein in the ipsilateral, but not in the contralateral, SSBF1 or the ipsilateral VPM at P8 after AAV-flex-TeLC.eGFP injection at E15.0. (**f–h**) Morphological analysis of Re^{+} interneurons after injection of AAV-flex-TeLC.eGFP in the absence (Ctrl, n = 9 interneurons) and presence (TeLC, n = 10

interneurons) of the *Emx1*^{Cre} allele. Since comparison of Re^{+} interneuron morphology after E15.5 and P0 injections did not show significant difference ($P > 0.05$), we pooled these groups for the analysis in **g** (axonal length: $P = 0.254$; axonal nodes: $P = 0.36$) and h (dendritic length: $P = 0.37$; dendritic nodes: $P = 0.548$). (**i**) A marked reduction of VAMP2 levels is observed in SSBF1 but not the striatum in *Emx1-TeLC* mice. (**j**) Intracortically evoked EPSCs recorded at −70 mV in layer I interneurons in a *TeLC* mouse (top) and in the *Emx1-TeLC* mouse (bottom). The red trace shows a small response that was obtained upon moving the stimulating electrode from layer II to layer I in the latter mice. (**k**) Average EPSC amplitude at −70 mV in layer I interneurons after stimulating layer II in control *TeLC* and *Emx1-TeLC* mice (Ctrl = 14 cells; *Emx1-TeLC* $n = 4$ cells, $P = 0.0008$, Mann-Whitney test). (**l**) Representative reconstructions of biocytin filled Re^{+} interneurons in layer I. (**m**) Quantification of length of dendritic arbors and axonal trees (Ctrl $n = 14$ interneurons; *Emx1-TeLC* $n = 8$ interneurons; axonal length, $P = 0.725$; dendritic length: $P = 0.24$). (**n**) Reduction of cortical thickness in *Bhlhp5*$^{Cre/+}$;*Munc18*$^{fl/fl}$ compared to *Munc18*$^{fl/fl}$ control mice at P9. (**o**) Representative reconstructions of biocytin filled Re+ interneurons in layer I. (**p**) Quantification of length of dendritic arbors and axonal trees. (mean values ±s.e.m.; Ctrl $n = 10$ interneurons; *Bhlhp5*$^{Cre/+}$;*Munc18*$^{fl/fl}$, $n = 4$ interneurons; axonal length, $P = 0.486$; dendritic length, $P = 0.194$). ***$P < 0.001$. Unpaired *t*-test. Scale bars in **b** and **c**, 800 μm; in **d, f, i, n, l** and **o**, 50 μm; in **e**, 100 μm.

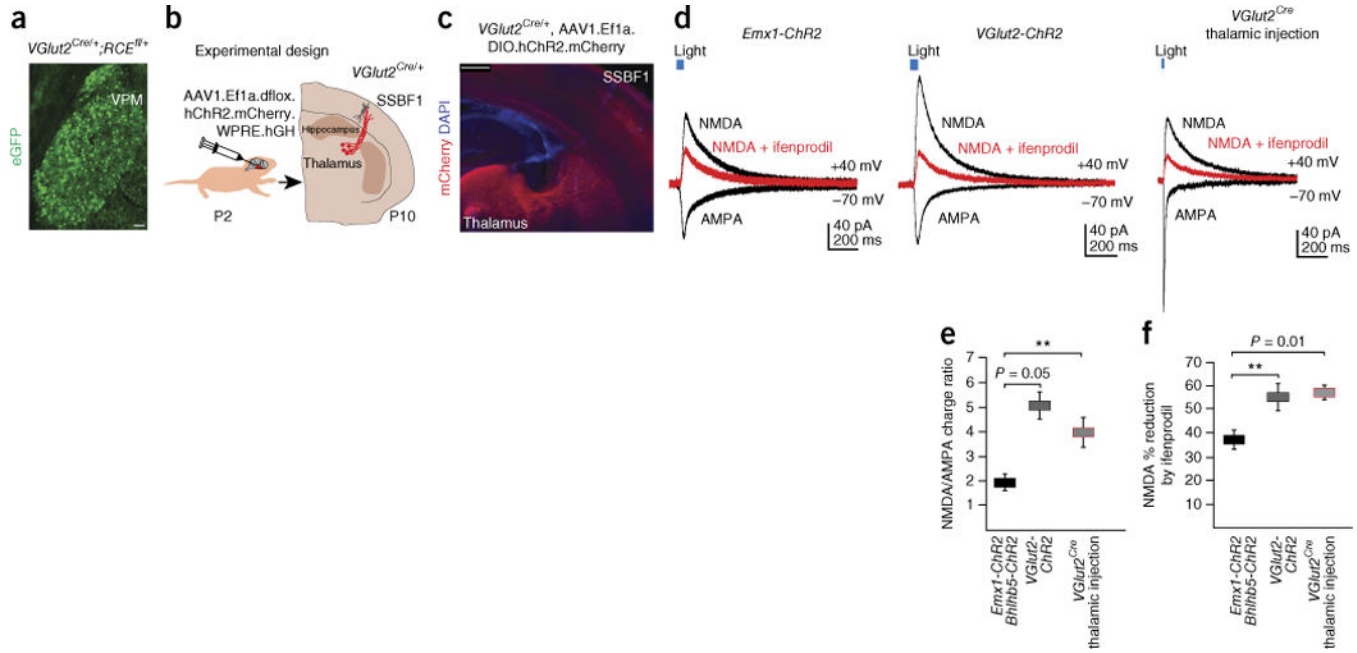

Figure 4.

Enrichment of NR2B-containing NMDARs activated by thalamic afferents onto Re^{+} interneurons. (**a**) eGFP expression in neuronal cell bodies in the VPM in $VGlut2^{Cre/+};RCE^{fl/+}$ (where RCE is an R26R CAG-boosted EGFP) mice. (**b**) Experimental design for viral injections. (**c**) A representative section of a thalamic injection showing mCherry expression in axons reaching SSBF1 in $VGlut2^{Cre/+}$-injected mice. (**d**) AMPAR- and NMDAR-mediated monosynaptic responses recorded from Re^{+} interneurons after light stimulation of $Emx1^{Cre+}$; $Rosa26^{LSL.ChR2\text{-}EYFP}$ or $Bhlhb5^{Cre/+};Rosa26^{LSL.ChR2.EYFP}$ (n = 11 interneurons), $VGlut2^{Cre/+};Rosa26^{LSL.ChR2.EYFP}$ (n = 12 interneurons) or $VGlut2^{Cre/+}$ thalamic injection (n = 9 interneurons) slices. Superimposed example traces of ifenprodil (3 μM) blockade of NMDAR mediated currents (red). (**e**) NMDAR/AMPAR charge ratio (±s.e.m.) (*Emx1-ChR2* versus *VGlut2-ChR2*, P = 0.0543; *Emx1-ChR2* versus $VGlut2^{Cre/+}$ thalamic injection, P = 0.0097, Mann-Whitney test). *Emx1-ChR2 Bhlhb5-ChR2* indicates that these data sets were pooled (see Online Methods). (**f**) The percentage reduction of NMDAR-dependent current amplitude after ifenprodil application (*Emx1-ChR2* versus VGlut2-ChR2, P = 0.0089; *Emx1-ChR2* versus $VGlut2^{Cre/+}$ thalamic injection, P = 0.0101, Mann-Whitney). **P < 0.01. Scale bar in **a**, 100 μm; in **c**, 500 μm. Error bars represent s.e.m.

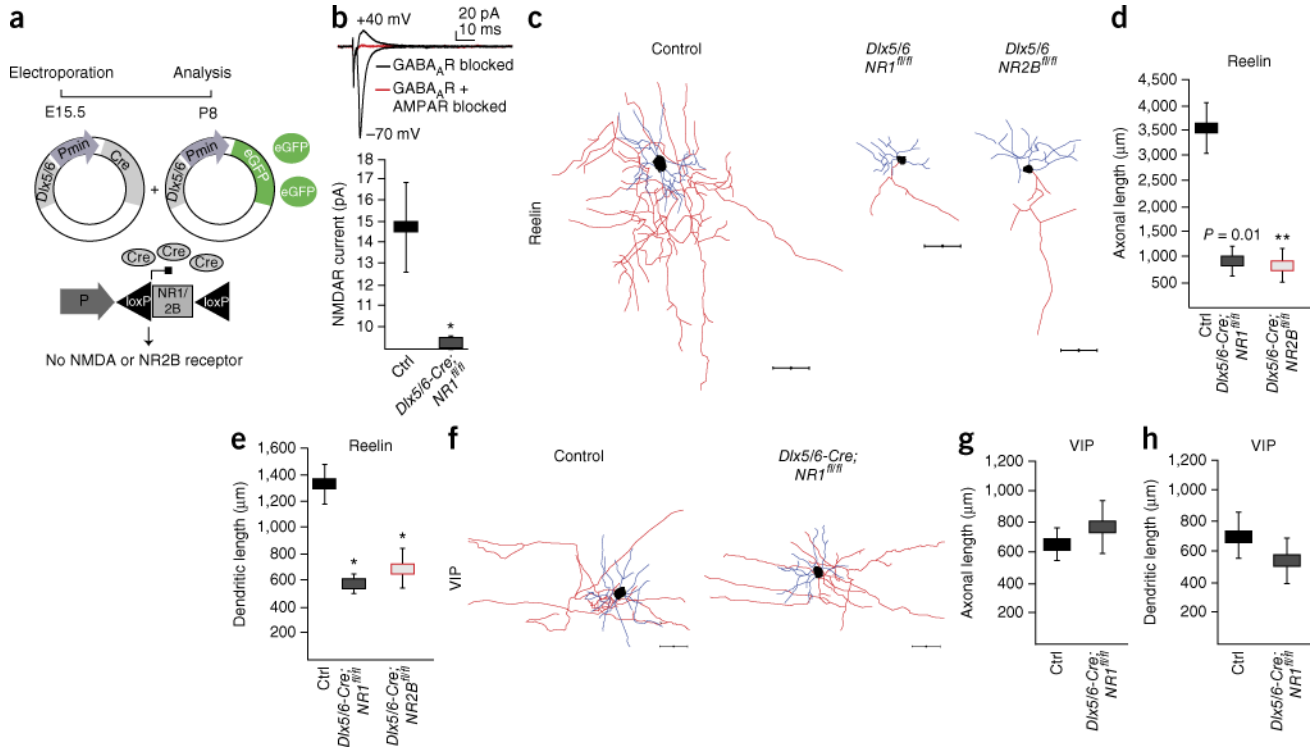

Figure 5.

NR2B-containing NMDARs are required for proper Re$^+$ but not VIP$^+$ interneuron development. (**a**) A schematic representation of the genetic strategy for ablation of NMDARs and NR2B-containing NMDARs in Re$^+$ interneurons. (**b**) The absence of NMDAR-mediated currents in *Dlx5/6-Cre;NR1*$^{fl/fl}$ cells and the presence of robust AMPAR-dependent currents (n = 7 control (Ctrl) interneurons (*NR1*$^{fl/fl}$) and n = 3 *Dlx5/6-Cre;NR1*$^{fl/fl}$ interneurons; Mann-Whitney test, P = 0.0167). $GABA_A$ receptors were blocked with SR95531. (**c–e**) Analysis of neuronal morphology in control (n = 25) interneurons (*NR1*$^{fl/fl}$ or *NR2B*$^{fl/fl}$) and in *Dlx5/6-Cre;NR1*$^{fl/fl}$ (n = 10) and *Dlx5/6-Cre;NR2B*$^{fl/fl}$ (n = 13) Re$^+$ interneurons (mean values ± s.e.m.; axonal length, *Dlx5/6-Cre;NR1*$^{fl/fl}$, unpaired t-test; P = 0.010; *Dlx5/6-Cre;NR2B*$^{fl/fl}$, P = 0.003; dendritic length, *Dlx5/6-Cre;NR1*$^{fl/fl}$, P = 0.020; *Dlx5/6-Cre;NR2B*$^{fl/fl}$, P = 0.016). (**f–h**) The same analysis performed in control (n = 9) and *Dlx5/6-Cre;NR1*$^{fl/fl}$ (n = 6) VIP$^+$ interneurons (axonal length, *Dlx5/6-Cre;NR2B*$^{fl/fl}$, P = 0.656; dendritic length: *Dlx5/6-Cre;NR1*$^{fl/fl}$, P = 0.678). *P < 0.05; **P < 0.01. Scale bars, 50 µm. Axons are shown in red, dendrites in blue.

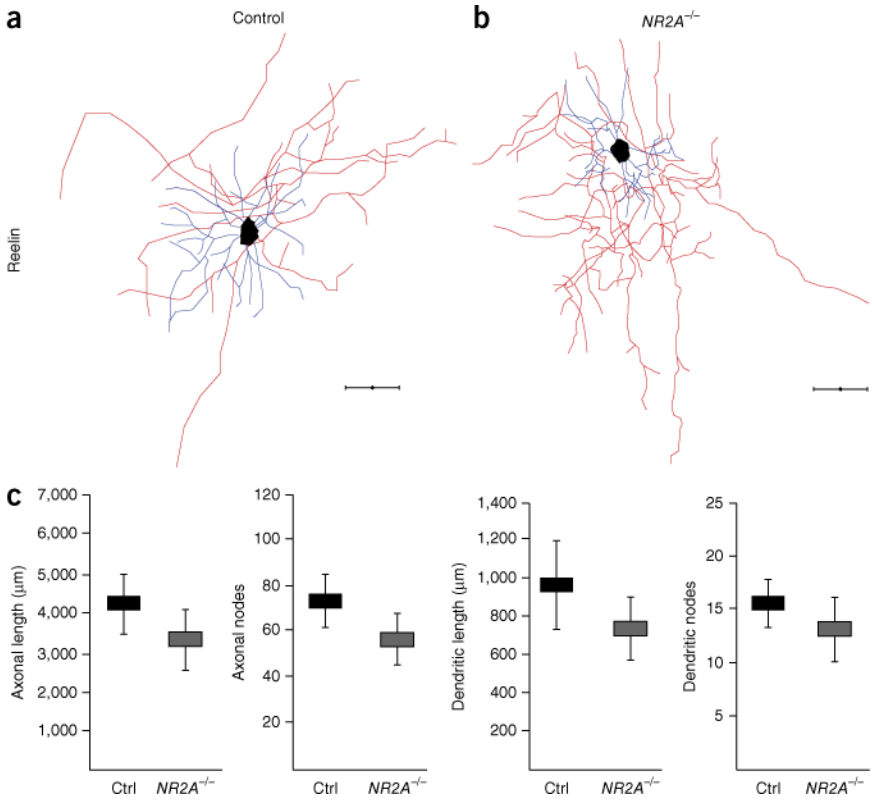

Figure 6.

Morphological development proceeds normally in *NR2A*$^{-/-}$ Re^{+} interneurons. (**a,b**) Neurolucida reconstructions of Re^{+} interneurons in control (**a**) and in *NR2A*$^{-/-}$ (**b**) mice. (**c**) Quantification of length and complexity of dendritic arbors and axonal trees (control (*NR2A*$^{+/+}$ and *NR2A*$^{+/-}$), $n = 7$ and *NR2A*$^{-/-}$, $n = 6$ interneurons; mean values ± s.e.m.; unpaired *t*-test; axonal length: $P = 0.345$; axonal nodes: $P = 0.243$; dendritic length: $P = 0.439$; dendritic nodes: $P = 0.272$). $P > 0.05$, ns. Scale bars, 50 µm. Axons are shown in red, dendrites in blue.

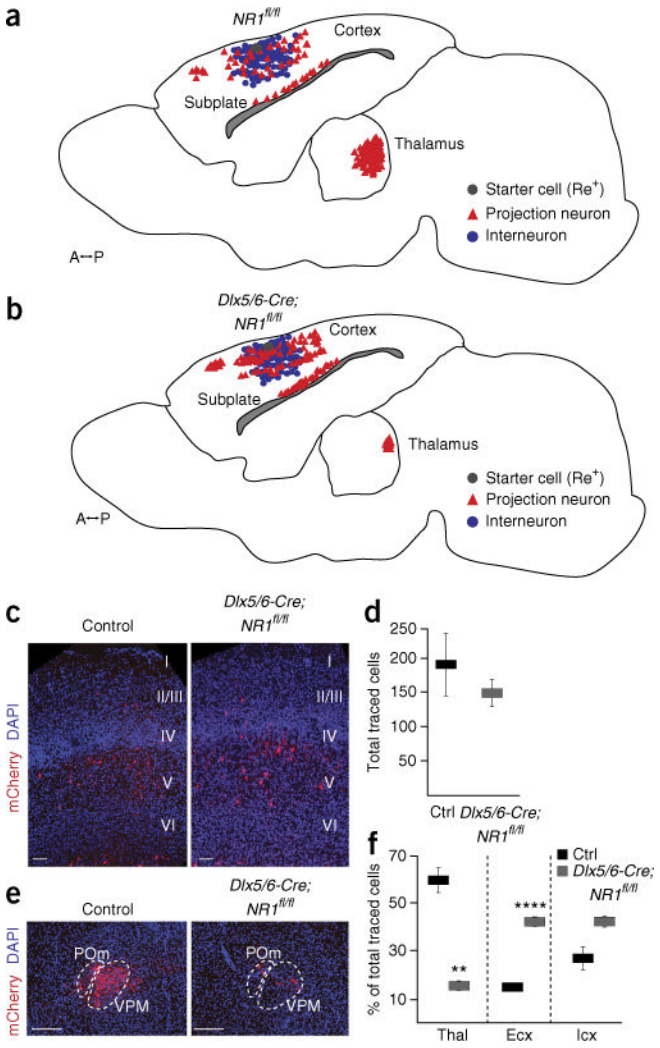

Figure 7.

NMDAR ablation reconfigures afferent connectivity onto Re^{+} interneurons. (**a,b**) The distribution of afferent inputs onto control (**a;** *Cre*$^{-}$, *NR1*$^{fl/fl}$) and *Dlx5/6-Cre;NR1*$^{fl/fl}$ (**b;** Cre^{+}, *NR1*$^{fl/fl}$) interneurons as revealed by monosynaptic rabies tracing (see Fig. 1a). (**c**) Representative images of cortical presynaptic neurons to control and *Dlx5/6-Cre;NR1*$^{fl/fl}$ interneurons. (**d**) Quantification of the total number of presynaptic neurons per starter cell in control (Ctrl; $n = 6$) and *Dlx5/6-Cre;NR1*$^{fl/fl}$ ($n = 3$) mice (mean values ± s.e.m.; unpaired *t*-test; $P = 0.646$). (**e**) Representative images of thalamic presynaptic neurons to control and *Dlx5/6-Cre;NR1*$^{fl/fl}$ interneurons. (**f**) The proportion of thalamic (Thal), cortical excitatory (Ecx) and cortical interneuron (Icx) inputs to control ($n = 6$ mice) and *Dlx5/6-Cre;NR1*$^{fl/fl}$ interneurons ($n = 3$ mice) (Thal, $P = 0.002$; Ecx, $P = 3.8E\text{-}06$; Icx, $P = 0.103$). $^{**}P < 0.01$; $^{****}P < 0.0001$. Scale bars in **c**, 50 μm; in **e**, 500 μm.